PNAS RESEARCH ARTICLE | BIOCHEMISTRY

Global profiling of arginine dimethylation in regulating protein phase separation by a steric effect–based chemical-enrichment method

Qi Wang[a,b,1], Zhouxian Li[a,c,1], Shenqing Zhang[d,1], Yichen Li[d], Yan Wang[a,b], Zheng Fang[a,b], Yanni Ma[a,b], Zhen Liu[a,b], Weibing Zhang[c], Dan Li[d,e], Cong Liu[b,f,g,2], and Mingliang Ye[a,b,2]

Edited by Benjamin Cravatt, The Scripps Research Institute, La Jolla, CA; received March 25, 2022; accepted September 20, 2022

Protein arginine methylation plays an important role in regulating protein functions in different cellular processes, and its dysregulation may lead to a variety of human diseases. Recently, arginine methylation was found to be involved in modulating protein liquid–liquid phase separation (LLPS), which drives the formation of different membraneless organelles (MLOs). Here, we developed a steric effect–based chemical-enrichment method (SECEM) coupled with liquid chromatography–tandem mass spectrometry to analyze arginine dimethylation (DMA) at the proteome level. We revealed by SECEM that, in mammalian cells, the DMA sites occurring in the RG/RGG motifs are preferentially enriched within the proteins identified in different MLOs, especially stress granules (SGs). Notably, global decrease of protein arginine methylation severely impairs the dynamic assembly and disassembly of SGs. By further profiling the dynamic change of DMA upon SG formation by SECEM, we identified that the most dramatic change of DMA occurs at multiple sites of RG/RGG–rich regions from several key SG-contained proteins, including G3BP1, FUS, hnRNPA1, and KHDRBS1. Moreover, both in vitro arginine methylation and mutation of the identified DMA sites significantly impair LLPS capability of the four different RG/RGG–rich regions. Overall, we provide a global profiling of the dynamic changes of protein DMA in the mammalian cells under different stress conditions by SECEM and reveal the important role of DMA in regulating protein LLPS and SG dynamics.

arginine dimethylation | chemical-enrichment method | RG/RGG motif | liquid–liquid phase separation | stress granule

Significance

Arginine methylation has been found to be important in regulating protein liquid–liquid phase separation (LLPS). Here, we developed a new chemoproteomics method for global profiling of arginine dimethylation (DMA) in modulating protein LLPS. We found that the sites within RG/RGG motifs are preferentially enriched in proteins of membraneless organelles (MLOs), especially stress granules (SGs). Importantly, the most dramatically changed DMA sites during SG formation localize in the RG/RGG–rich regions of several key SG-contained proteins, whose LLPS capabilities are significantly impaired by arginine methylation. By developing the new method, we revealed the essential role of DMA in regulating protein LLPS and paved the road for further study of protein DMA in other biological processes.

As one of the important protein posttranslational modifications, arginine methylation regulates the structural conformations and physiological functions of a variety of proteins involved in different biological processes, such as transcription regulation, pre–messenger RNA (pre-mRNA) splicing, and the DNA damage response (1–3). Dysregulation of arginine methylation is closely associated with diseases such as cancer and neurodegenerative diseases (4–9). Recently, mounting evidence has demonstrated that arginine methylation may play an important role in regulating liquid–liquid phase separation (LLPS) of the proteins involved in the dynamic (dis)assembly of different membraneless organelles (MLOs) (8–11). Moreover, dysregulations of LLPS of several disease-related proteins, including FUS and TDP-43, are closely related to different neurodegenerative diseases (12), implying a possible link between arginine methylation of pathological proteins for regulating LLPS and diseases (8, 9). Methylation can directly alter the hydrophobicity and the hydrogen-bonding ability of the side chain of arginine residue, and thus weaken the cation-π interaction essential in mediating protein LLPS (10, 13–15). Although arginine methylation has been found to modulate LLPS of several individual proteins, the global identification and characterization of arginine methylation in regulating protein LLPS and MLO dynamic assembly were still lacking.

Methylated arginine features three different forms including monomethylated arginine (MMA), asymmetrical dimethylated arginine (aDMA), and symmetrical dimethylated arginine (sDMA), which are regulated by nine different protein arginine methyltransferases (PRMTs). To analyze the three different forms at the proteome level, a series of different strategies were developed (16–23). Among them, the immunoaffinity-based enrichment method exhibits the best performance in the identification of both MMA and DMA. But in comparison with MMA identification, its performance in DMA identification is relatively poor (18). Since aDMA or sDMA generated from MMA has been found to play a crucial role in fulfilling different functions in many biological processes (1, 4), it would be important to develop a robust method specifically for the global profiling of DMA sites at the proteome level.

The authors declare no competing interest.

This article is a PNAS Direct Submission.

[1]Q.W., Z. Li, and S.Z. contributed equally to this paper.

[2]To whom correspondence may be addressed. Email: mingliang@dicp.ac.cn or liulab@sioc.ac.cn.

This article contains supporting information online at http://www.pnas.org/lookup/suppl/doi:10.1073/pnas.2205255119/-/DCSupplemental

Published October 18, 2022.

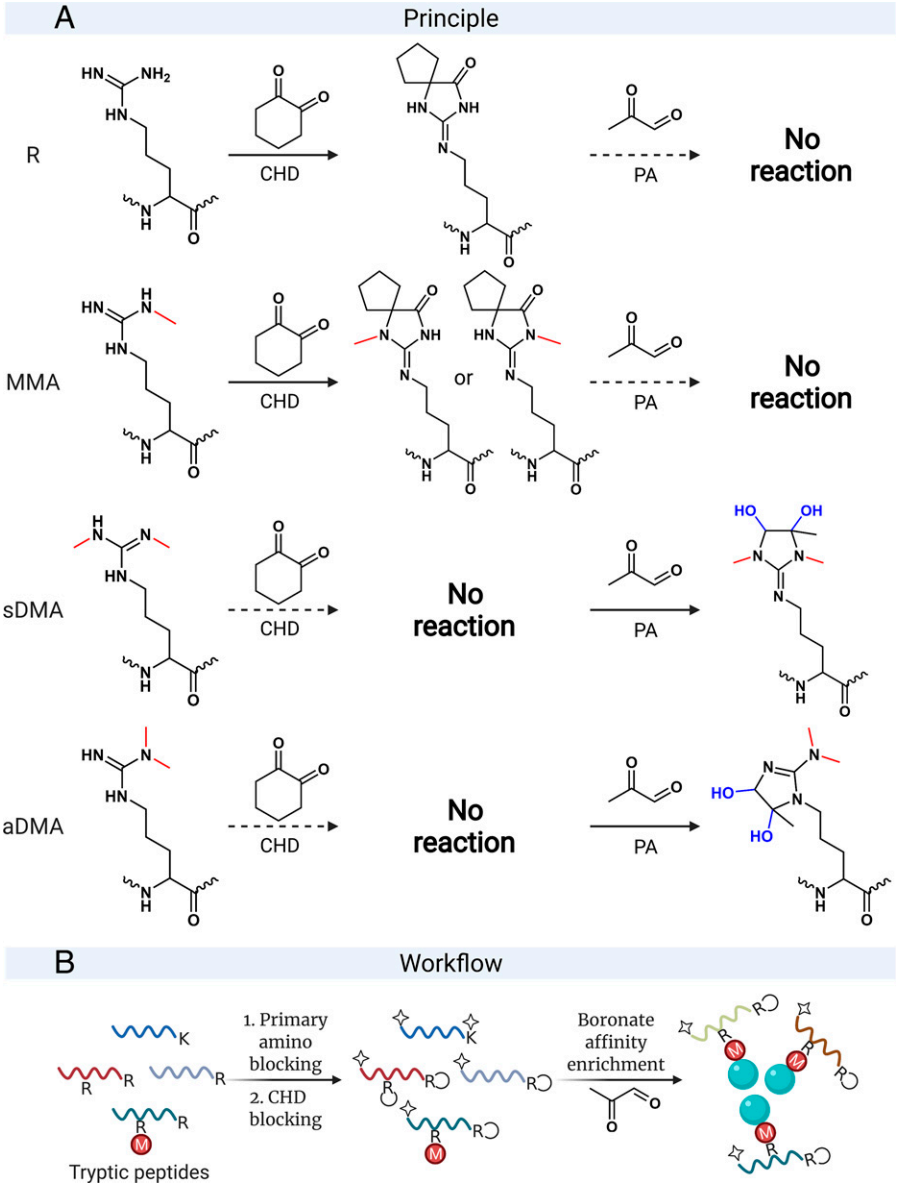

Fig. 1. Design of SECEM to enrich arginine dimethylated peptides. (*A*) Principle for the selective derivatization of dimethylated arginine residue with *cis*-diol. Briefly, unmethylated arginine residue or MMA selectively reacts with 1,2-cyclohexanedione (CHD) to form a spirocyclic group, which prevents them from reacting with pyruvic aldehyde (PA), while aDMA or sDMA that cannot react with CHD would further react with PA to form a *cis*-diol, enabling boronate affinity enrichment. (*B*) Workflow of SECEM. The primary amino-blocked peptide mixture is treated with CHD to block the un- and monomethylated arginine residues. Then dimethylated arginine residues in the obtained sample are modified with *cis*-diol by PA and further enriched by using boronate-affinity chromatography (refer to *SI Appendix*, Fig. S6 for the detailed information). The block group labeled on the primary amino is represented by a star, the spirocyclic structure by a semicircle, DMA by "R" labeled with "M," and boronate-modified resin for the boronate-affinity chromatography by green spheres.

Here, we developed a steric effect–based chemical-enrichment method (SECEM), a chemistry method which can enrich arginine dimethylated peptides from complex peptide mixtures (Fig. 1 *A* and *B*). Compared with the immunoaffinity-enrichment method, our method largely increases the enrichment efficiency and features superior performance in identifying the DMA sites within the RG/RGG motif. Comprehensive analysis of the DMA data set identified by SECEM suggests that DMA within the RG/RGG motif is closely implicated in stress granules (SGs). Thus, we further analyzed its dynamic change upon SG formation in cells and performed a series of in vitro assays to explore how arginine methylation of the RG/RGG motif regulates protein LLPS. Overall, our work highlights the importance of the arginine methylation within the RG/RGG motif in modulating protein LLPS and the dynamic assembly of SGs.

Results

Design of SECEM. Boronate-affinity chromatography, based on the reversible covalent interaction between boronate and *cis*-diol, was broadly used to enrich various *cis*-diol–containing compounds such as carbohydrates, nucleotides, and glycoproteins (24). Because the guanidine group on an arginine residue can be modified with a *cis*-diol group by reacting with vicinal dicarbonyl compound, boronate-affinity chromatography was also applied to enrich arginine-containing peptides (25–27). Inspired by this strategy, we designed a chemical method to specifically enrich arginine-dimethylated peptides.

Arginine residue can react with 1,2-cyclohexanedione to form a spirocyclic structure (27). In this study, we found that both unmethylated and monomethylated arginine residues can react with 1,2-cyclohexanedione, while the dimethylated arginine

residue in the form of either aDMA or sDMA remained unchanged (*SI Appendix*, Fig. S1). Meanwhile, the reaction is quite complete, as only ∼0.23% of peptides carrying unmethylated arginine residue from the digest of whole protein were not modified (*SI Appendix*, Table S1). Because the steric hindrance of this spirocyclic structure is much larger than the dimethyl group, we hypothesized that pyruvic aldehyde preferentially reacts with dimethylated arginine residue rather than the spirocyclic structure–modified un- or monomethylated arginine residue to form a *cis*-diol group (Fig. 1*A*). On that basis, we designed the SECEM to enrich arginine dimethylated peptides (Fig. 1*B*). As expected, SECEM could enrich the arginine dimethylated peptides in the form of either aDMA or sDMA from the peptides carrying un- or monomethylated arginine residue (*SI Appendix*, Figs. S2 and S3).

Next, we sought to evaluate the enrichment performance of SECEM. The synthetic tryptic peptide carrying aDMA or sDMA was mixed with the tryptic digest of bovine serum albumin (BSA) at the mass ratio of 1:100 to mimic the real tryptic digest of whole proteins in cells, and then was enriched by SECEM. Strikingly, both aDMA- and sDMA-carrying peptides were successfully enriched (Fig. 2). Even though the mass ratio was increased to 1:1,000, both arginine dimethylated peptides were enriched with high selectivity (*SI Appendix*, Fig. S4). Taken together, SECEM, designed by exploiting the steric hindrance of the spirocyclic group, can enrich arginine dimethylated peptide in the form of either aDMA or sDMA with good performance.

Proteomics Profiling of Arginine Dimethylation in Mammalian Cells by SECEM. Because the mass shifts caused by methylation are identical to the mass differences between many amino acid residues, the large-scale mass spectrometry (MS)–based identification of methylpeptides is proven to have a high false-positive rate (28, 29). To control DMA identification confidence, we applied a method by coupling metabolic labeling of "heavy" methionine with an algorithm called IonPEP in this study (detailed in *Materials and Methods*; *SI Appendix*, Fig. S5). We applied SECEM to enrich arginine dimethylated peptides from 100 μg of tryptic digest of the whole protein in mammalian Jurkat T cells (a detailed workflow is presented in *SI Appendix*, Fig. S6). On average, 184 arginine dimethylated peptides were identified in a single MS run (Fig. 3*A*). In contrast to directly analyze the whole-protein digest, the number of identified arginine dimethylated peptides was increased by 5.13 times, and the number of identified DMA sites by 5.16 times.

However, we noticed that 85.79% of the peptides not carrying DMA still have at least one arginine residue after the enrichment, while the percentage of arginine-containing peptides is only 46.10% for the direct analysis of the tryptic digest of whole proteins (*SI Appendix*, Table S2). Thus, arginine residues modified by 1,2-cyclohexanedione still have little chemical activity to react with pyruvic aldehyde and are then partially enriched by boronate-affinity chromatography. To identify more DMA sites, we further improved the sample preparation scheme to reduce the proportion of arginine-containing peptides. Because the dimethylation of arginine could inhibit the protease cleavage on this residue, DMA sites are always presented in the middle of tryptic peptides (16, 20–22). In comparison, unmethylated arginine residues are mainly presented in the C terminuses. Thus, unmethylated arginine residues can be selectively cut off by carboxypeptidase B, an exopeptidase cutting the basic amino acid residue in peptide C terminus. In addition, we also found that 11.69% of arginine-containing peptides carry the unmethylated arginine residue in the peptide middle due to the missed cleavage in the process of trypsin digestion. To expose more unmethylated arginine residues to the peptide C terminus, the tryptic digest was further digested

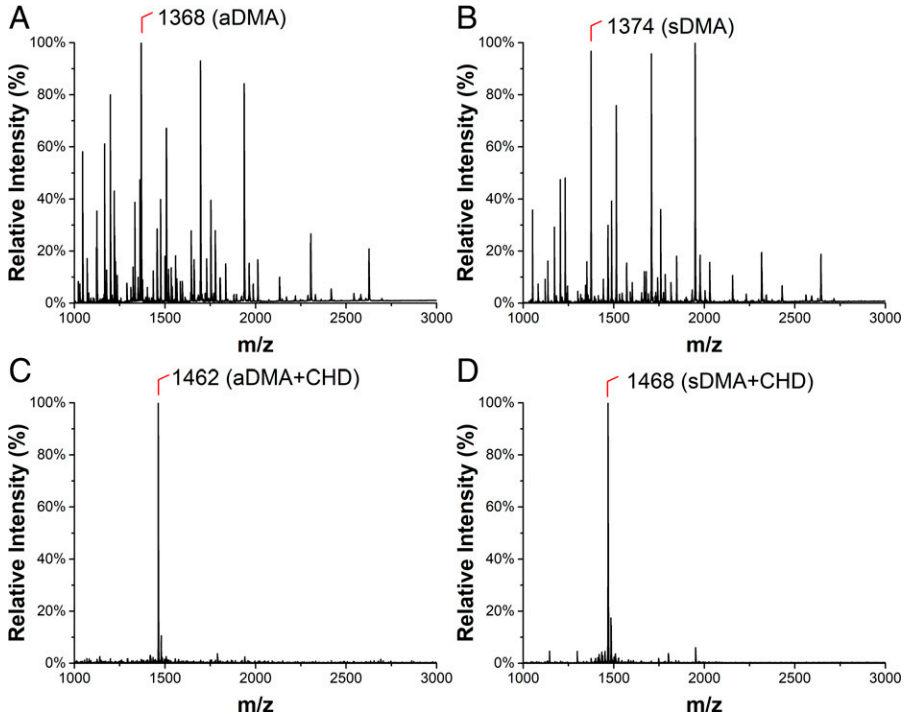

Fig. 2. SECEM enables selective enrichment of arginine dimethylated peptide from a peptide mixture. The peptide mixture included an arginine dimethylated peptide, GGNFSG-aDMA-GGFGGSR or GGNFSG-sDMA-GGFGGSR, and the tryptic digest of BSA at a mass ratio (*m/z*) of 1:100. (*A* and *B*) The aDMA- or sDMA-carrying peptide was observed with a very noisy background when the peptide mixture was directly analyzed by MALDI MS, while a dominant peak with a clean background (*C* and *D*) was observed after the enrichment. Note that the unmethylated arginine residues in the C terminuses of both arginine dimethylated peptides were modified by 1,2-cyclohexanedione (CHD), which caused the mass shift of +94 Da.

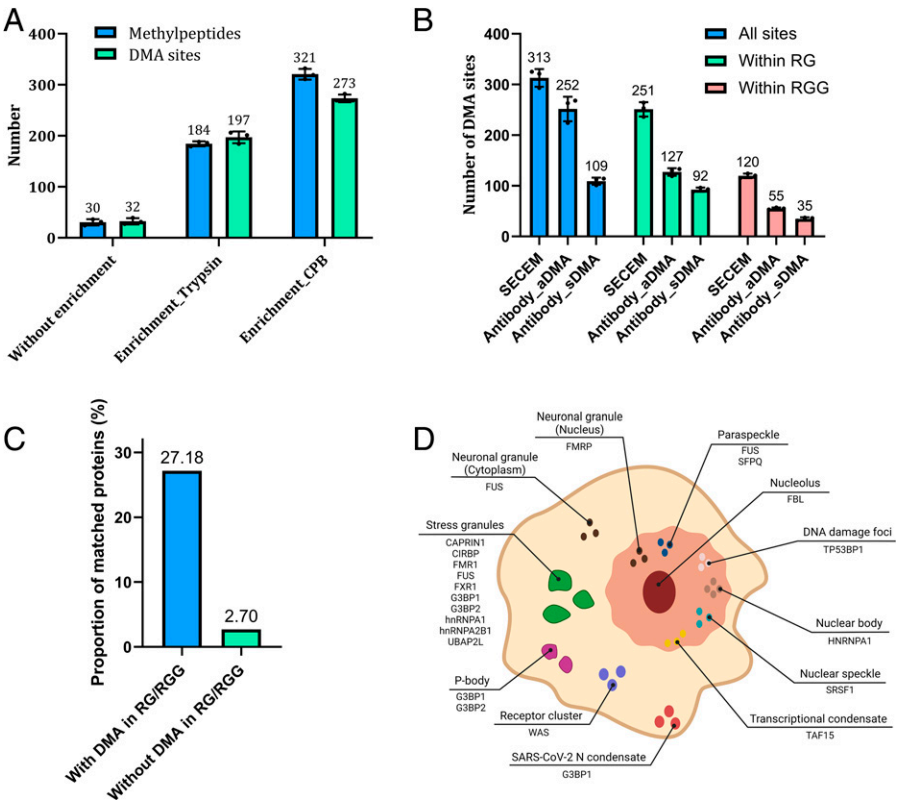

Fig. 3. Identification performance of SECEM and bioinformatics analysis of the identifications. (*A*) The number of DMA sites identified from Jurkat T cells by using SECEM coupled with different protein digestion strategies. Peptides (100 μg) were used as starting material for each enrichment experiment. "Without enrichment" refers to the direct analysis of the tryptic digest without the enrichment. "Enrichment_Trypsin" means that the protein sample was digested by trypsin alone before SECEM enrichment. "Enrichment_CPB" means that the protein sample was digested by trypsin, ArgC, and carboxypeptidase B (CPB) before SECEM enrichment. Data were repeated in triplicate for each bar. Error bars indicate SD. (*B*) The number of the DMA sites within different motifs identified by using different enrichment methods. Peptides (200 μg) were used as starting material for each SECEM enrichment experiment, while 10 mg of proteins was used as starting material for each immunoaffinity-enrichment experiment. Data were repeated in triplicate for each bar. Error bars indicate SD. (*C*) The proportion of arginine methylated proteins presented in the database consisting of LLPS-regulating proteins. The arginine dimethylated proteins identified by using SECEM were separated into two groups according to whether the protein carries the identified DMA sites within the RG/RGG motif, and matched to the database. (*D*) Distribution of the database-matched proteins in different MLOs. All the proteins labeled in this cellular schematic carry the identified DMA sites within the RG/RGG motif.

by Arg-C, a protease having better efficiency cutting arginine residues than trypsin. As expected, the proportion was decreased to 3.10%. The resulting digest was then treated with carboxypeptidase B. Dramatically, the proportion of arginine-containing peptides was decreased from 45.02% to 6.67% (*SI Appendix*, Table S2). Arginine dimethylated peptides were then enriched by SECEM. Strikingly, by using this optimized sample preparation method, the number of identified arginine dimethylated peptides was increased from 184 to 321, and the number of identified DMA sites from 197 to 273 (Fig. 3*A*). When the starting amount of peptide was increased from 100 μg to 200 μg, the numbers of identified arginine dimethylated peptides and DMA sites were further increased to 375 and 313, respectively (Fig. 3*B* and *SI Appendix*, Fig. S7).

Immunoaffinity enrichment is a frequently used method to enrich arginine methylated peptides (17–19, 30, 31). Two different antibodies were developed to enrich aDMA- and sDMA-carrying peptides, respectively. To compare their performance with SECEM, we used these two antibodies to enrich the arginine dimethylated peptides from the whole-protein digest of Jurkat T cells. On average, 252 and 109 DMA sites were identified in one liquid chromatography–mass spectrometry run by using aDMA and sDMA antibodies, respectively (Fig. 3*B*). It should be noted that the data were obtained by using 10 mg of proteins in each immunoaffinity-enrichment experiment according to the recommended protocol (31). When the sample amount was decreased to 200 μg of peptides, as SECEM used, the identified numbers by using aDMA and sDMA antibodies were sharply decreased to 39 and 29, respectively (*SI Appendix*, Fig. S7). Clearly, SECEM has much higher efficiency to enrich dimethylated peptides. In comparison with the identifications obtained by using immunoaffinity enrichment with 10 mg of proteins, SECEM exhibits superior performance in identifying DMA sites within the RG/RGG motif (Fig. 3*B* and *SI Appendix*, Fig. S8). The number of identified DMA sites within the RG motif was increased by >97.64%, and the number of DMA sites within the RGG motif was increased by >118.18%.

The RG/RGG motif is widely presented in proteins and regulates various biological processes such as DNA damage, gene transcription, pre-mRNA splicing, mRNA translation, and the apoptosis pathway by mediating protein–protein and RNA–protein interactions (32, 33). Recently, mounting evidence also has shown that the RG/RGG motif is crucial to regulate protein LLPS (8, 9, 33–36). Considering the importance of the RG/RGG motif in biology, we performed a series of bioinformatics analyses for the DMA sites within the RG/RGG motif identified by SECEM. Strikingly, in silico prediction shows that 94.82% of these sites are localized in the intrinsically disordered regions (IDRs). Since the IDRs were found to play an important role in modulating protein LLPS in different MLOs (37–39), we next sought to assess whether the proteins with identified DMA sites are identified or predicted to undergo

LLPS or are involved in different MLOs. Notably, when we matched proteins carrying the DMA site(s) within the RG/RGG motifs to the database (40), 27.18% of proteins were annotated as LLPS-regulating proteins (Fig. 3*C*). Moreover, 16 of 28 matched proteins are involved in the formation of 12 different MLOs, including SGs, P-body, and paraspeckles (Fig. 3*D*). In contrast, the percentage is only 2.7% for SECEM-identified arginine dimethylated proteins not carrying the DMA site within the RG/RGG motif (Fig. 3*C*). Taken together, our results strongly suggest that the DMA sites within the RG/RGG motif are closely associated with protein LLPS involved in different MLOs.

Global Inhibition of Arginine Methylation Promotes SG Formation and Impairs Self-Disassembly of SGs. Our data show that 10 of 16 MLO-related methylproteins identified by SECEM are implicated in SGs, implying that DMA plays an important role in SG regulation (Fig. 3*D*). We thus examined whether the global change of protein arginine methylation influences SGs assembly and disassembly in HeLa cells. Global down-regulation of protein arginine methylation level was achieved by treating cells with the combination of type I PRMT inhibitor and PRMT5 inhibitor (i.e., MS023 and GSK591) (*SI Appendix*, Fig. S9). Notably, upon stress induced by sodium arsenite, we observed that both the average number and the mean area of SGs per cell were significantly increased in the inhibitor-treated cells (Fig. 4 *A*–*C*), which is consistent with previous observation in U2OS cells (11).

We further asked whether the inhibition of global protein arginine methylation level influences the dynamics disassembly of SGs. We performed a washout assay in stressed HeLa cells by removing the sodium arsenite in the culture medium. In the controlled cells, the average number of SGs per cell was dramatically decreased by ∼70.5%, and the average area of SGs per cell was decreased by ∼79.9% (Fig. 4 *D*–*F*). Whereas, in the inhibitor-treated cells, the average number and the mean area were only decreased by 19.8% and 37.5%, respectively. Therefore, the dynamic disassembly of SGs is severely impaired upon the inhibitor treatment. Taken together, our results demonstrate that inhibition of global protein arginine methylation significantly facilitates the formation of SGs as well as diminishes the disassociation of SGs in HeLa cells.

Methylproteome Analysis Reveals the Dynamic Change of Arginine Dimethylation Upon SG Formation. We next analyzed the change of DMA, especially DMA within the RG/RGG motif, at the proteome level during SG formation by using SECEM (Fig. 5*A*, detailed in *Materials and Methods*). We induced SG formation by treating cells with different stress conditions, including sodium arsenite treatment and heat shock. As for sodium arsenite treatment, 280 arginine dimethylated peptides in 92 proteins were identified, and the abundance of 16 arginine dimethylated peptides in 15 proteins was changed (Fig. 5*B* and *SI Appendix*, Table S3). Notably, among the identified proteins, nine proteins are annotated in the RNA granule database as being included in SGs, and three proteins (i.e., hnRNPR, KIF1C, and NCL) are predicted to exhibit LLPS capability (41) (Fig. 5*C*). For heat-shock treatment, 226 arginine dimethylated peptides were identified from 77 proteins, and seven methylpeptides in seven proteins were significantly changed upon the stress (Fig. 5*D* and *SI Appendix*, Table S3). Among them, five proteins are presented in SGs (Fig. 5*E*).

Strikingly, the DMA levels of several well-known SG components, including the crucial SG scaffold protein G3BP1 (42), and FUS and hnRNPA1, exhibit significant changes under both stress conditions (Fig. 5 *C* and *E*). The changed methylpeptides under both stress conditions were identical for all three proteins (*SI Appendix*, Table S4). Moreover, these methylpeptides are all localized in the RG/RGG–rich regions, which are IDRs and were previously characterized to be crucial for mediating protein LLPS (9, 42–46) (*SI Appendix*, Figs. S10 and S11 and Table S4). Besides these three proteins, KHDRBS1, which was previously reported to be recruited into SGs, was also identified in both stress conditions (*SI Appendix*, Table S4). And the identified methylpeptide is also located in an RG-rich region, which is an IDR vital for KHDRBS1 to localize into SGs (47, 48) (*SI Appendix*, Figs. S10 and S11). Of note, as arginine methylation inhibits trypsin digestion, the change of arginine dimethylated peptide may be caused by the change of methylation state on the arginine residue within this peptide or ahead of the N terminus of this peptide (*SI Appendix*, Fig. S12). Here, we defined the sequence containing those two types of arginine methylated sites as the region with changed arginine methylation (RCAM). We found 11 potential changed DMA sites in the RCAMs of the four RG/RGG–rich regions (*SI Appendix*, Fig. S10). Taken together, our results demonstrated the DMA within the IDRs of the key SG-containing proteins are dynamically regulated upon the SG formation.

Arginine Methylation of the RG/RGG–Rich Region Is Crucial in Regulating Protein LLPS. Next, we sought to evaluate whether arginine methylation effects LLPS of the RG/RGG–rich regions (*SI Appendix*, Table S5 and Fig. S13). We overexpressed and purified four different RG/RGG–rich regions, respectively. Consistent with previous studies, the RG/RGG–rich regions of G3BP1, FUS, and hnRNPA1 are highly prone for undergoing LLPS (*SI Appendix*, Fig. S14). Notably, the RG-rich regions of KHDRBS1 also exhibits potent LLPS capability and forms liquid-like droplets in vitro. We then set up an in vitro arginine methylation assay by using PRMT1 from rat (i.e., Prmt1). PRMT1 is the major asymmetric arginine methyltransferase in mammalian (4) and was previously identified to interact with three of these four RG/RGG–containing proteins from a PRMT interactome study (49). By using matrix-assisted laser desorption/ionization mass spectrometry (MALDI-MS), we confirmed that the four RG/RGG–rich regions were methylated by Prmt1 (*SI Appendix*, Fig. S15). Moreover, we used LC-MS/MS to further identify 26 DMA sites on the four different RG/RGG–rich regions (*SI Appendix*, Fig. S15 *A*–*D*). Notably, we validated that most of the DMA sites ($n = 9$ of 11) identified from our cell assays are modified by Prmt1 in the in vitro pure protein assay.

We then examined how arginine methylation influences LLPS of these four RG/RGG–rich regions by preparing five different samples for each RG/RGG–rich region (*SI Appendix*, Table S5 and Fig. S13). Importantly, we found that Prmt1-mediated arginine methylation significantly impairs LLPS of all four RG/RGG–rich regions (Fig. 6), whereas blocking enzymatic activity of Prmt1 by an inhibitor MS023 abolishes the inhibitory effect on protein LLPS. As a control, *S*-adenosylmethionine, the substrate of arginine methylation reaction, does not influence LLPS of the four RG/RGG–rich regions (*SI Appendix*, Fig. S16). In addition, we mutated the 11 arginine residues identified in RCAMs to alanine in the four RG/RGG–rich regions. Strikingly, all four mutants exhibited severely impaired capability for LLPS in vitro, which further validates the important role of these arginine residues in mediating LLPS of the RG/RGG–rich regions (*SI Appendix*, Fig. S17).

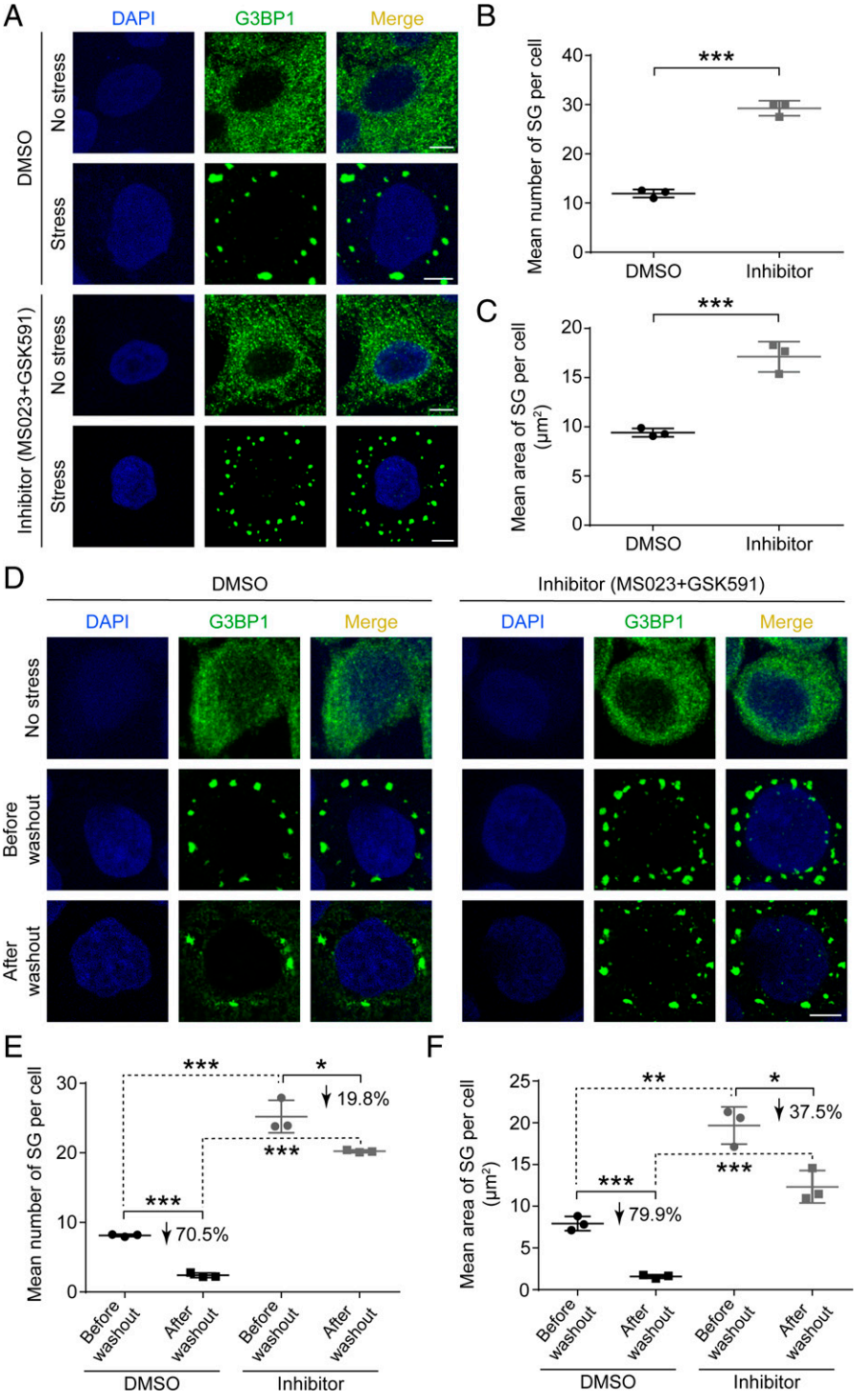

Fig. 4. Globally decreasing arginine methylation promotes the assembly of SGs and impairs the disassembly of SGs. (*A*) Confocal images of the SG assembly in HeLa cells. Cells were treated with DMSO or PRMT inhibitors and then stressed by sodium arsenite. The nucleus was stained with blue, and G3BP1 with green. Scale bar: 5 μm. (*B* and *C*) Quantification analysis of the images in *A*. Error bars indicate SD, and >150 cells from three replicates were counted for each bar. (*D*) Confocal images of the SG disassembly in HeLa cells. Cells were treated with DMSO or inhibitors first. Sodium arsenite was used to stimulate the SG assembly of cells and followed by washing out. Nucleus was stained with blue, and G3BP1 with green. Scale bar: 5 μm. (*E* and *F*) Quantification analysis of the images in *D*. Error bars indicate SD, and >150 cells from three replicates were counted for each bar. $^{*}P < 0.05$, $^{**}P < 0.01$, $^{***}P < 0.001$ by Student's *t* test.

Discussion

In this study, we developed a chemical-enrichment method, SECEM, to selectively enrich arginine dimethylated peptides from protein digest. As a chemical method, the enrichment of SECEM is not much influenced by the types of residues adjacent to the methylation sites. Thus, SECEM can identify DMA next to almost all kinds of natural amino acid residues and within the different motifs, including several common motifs reported previously (i.e., RXR, RXXY, and proline-rich motifs) (17, 19) (*SI Appendix*, Fig. S18). In comparison, methylation-specific antibodies were developed by using a methylated-peptide library with specific motifs as the antigen. Since the glycine residue without bulky side chain has very limited

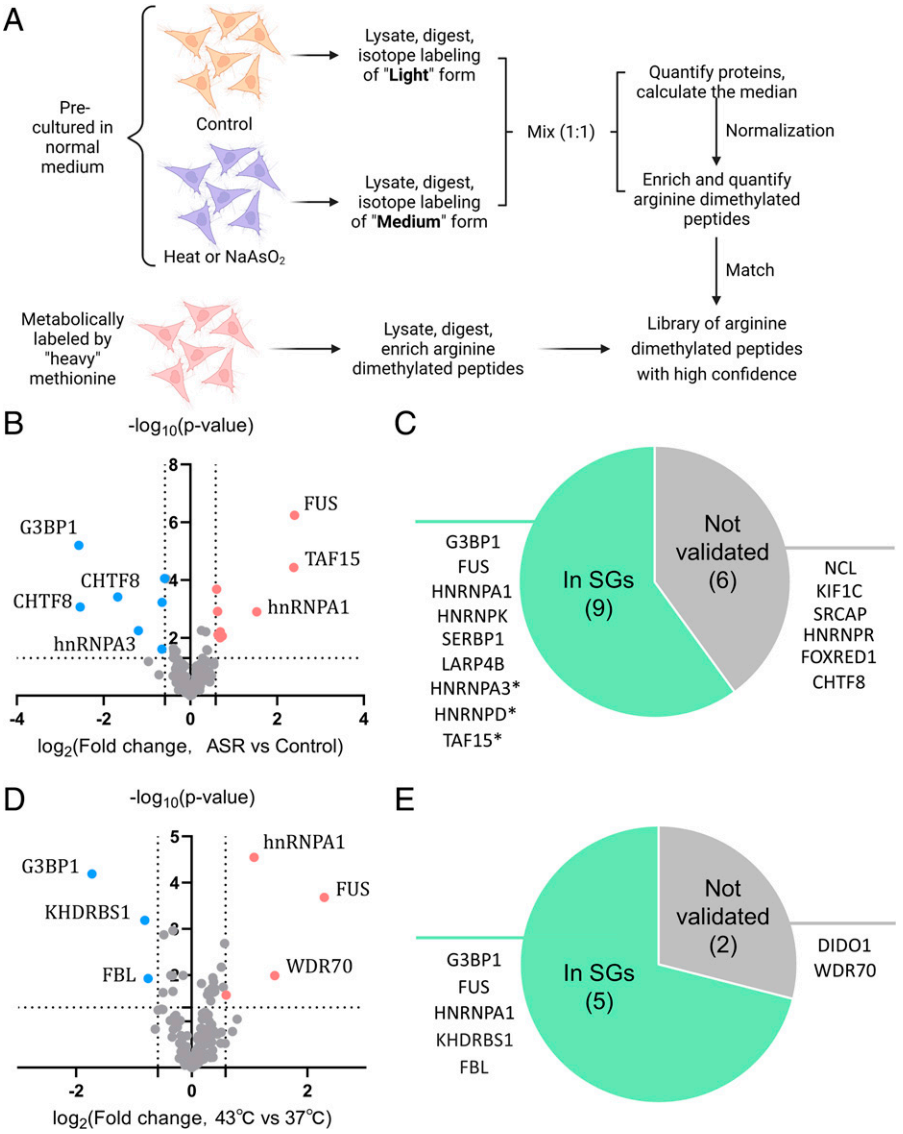

Fig. 5. Profiling the dynamic change of DMA in HeLa cells under the stress of sodium arsenite (ASR) or heat shock. (*A*) Workflow of the methylproteome analysis. (*B*) Volcano plot illustrating the change of arginine dimethylated peptides for HeLa cells under the stress of ASR treatment (n = 5 biological replicates). Significantly changed arginine dimethylated peptides with >1.5-fold change and $P < 0.05$ are labeled with red or blue. P value was calculated by Student's t test. (*C*) The proportion of the labeled proteins from *B* in SGs. The proteins labeled by an asterisk are the SG proteins predicted in the RNA granule database. (*D*) Volcano plot illustrating the change of arginine dimethylated peptides for HeLa cells under the stress of heat shock (n = 4 biological replicates). Significantly changed arginine dimethylated peptides with >1.5-fold change and $P < 0.05$ are labeled with red or blue. P value was calculated by Student's t test. (*E*) The proportion of the labeled proteins from *D* in SGs.

contribution to the enrichment, the immunoaffinity method exhibits less capability for enriching DMA within the RG/RGG motif than SECEM.

It is worth noting that although SECEM can identify DMA sites within various motifs, not all DMA sites identified by the immunoaffinity method were included in the dataset of SECEM (*SI Appendix*, Fig. S8). Additional experiments are needed to find out why these sites were not identified by SECEM. The methyl-specific antibodies developed in an immunoaffinity method could also be used to probe the arginine dimethylation at the protein level and have broad applications in assays such as Western blotting and immunohistochemistry. Currently, SECEM was developed and optimized to enrich DMA peptides for proteomics analysis. Theoretically, it also works for probing arginine dimethylation at the protein level; however, its performance needs further investigation.

In the dataset of SECEM-identified DMA sites, we found that the DMA sites within the RG/RGG motif rather than other motifs are preferentially enriched in the proteins implicated in MLOs, especially SG. More importantly, our SECEM study further pinpointed the dramatic change of the DMA of several SG-containing proteins, including G3BP1, FUS, hnRNPA1, and KHDRBS1 upon SG formation. This suggests that the dynamic regulation of DMA on SG-containing proteins is crucial for modulating SG assembly and disassembly. Indeed, the global inhibition of protein arginine methylation significantly promotes SG formation and severely impairs SG disassembly. It will be interesting to further explore whether arginine methylation is dynamically regulated for proteins involved in other MLOs, such as P-body, paraspeckle, and TDP-43 nuclear body, for fine-tuning their dynamic assembly and disassembly.

Materials and Methods

Enrichment of Synthetic Arginine Dimethylated Peptides. The four peptides sharing the same sequence (i.e., GGNFSGRGGFGGS), but with different

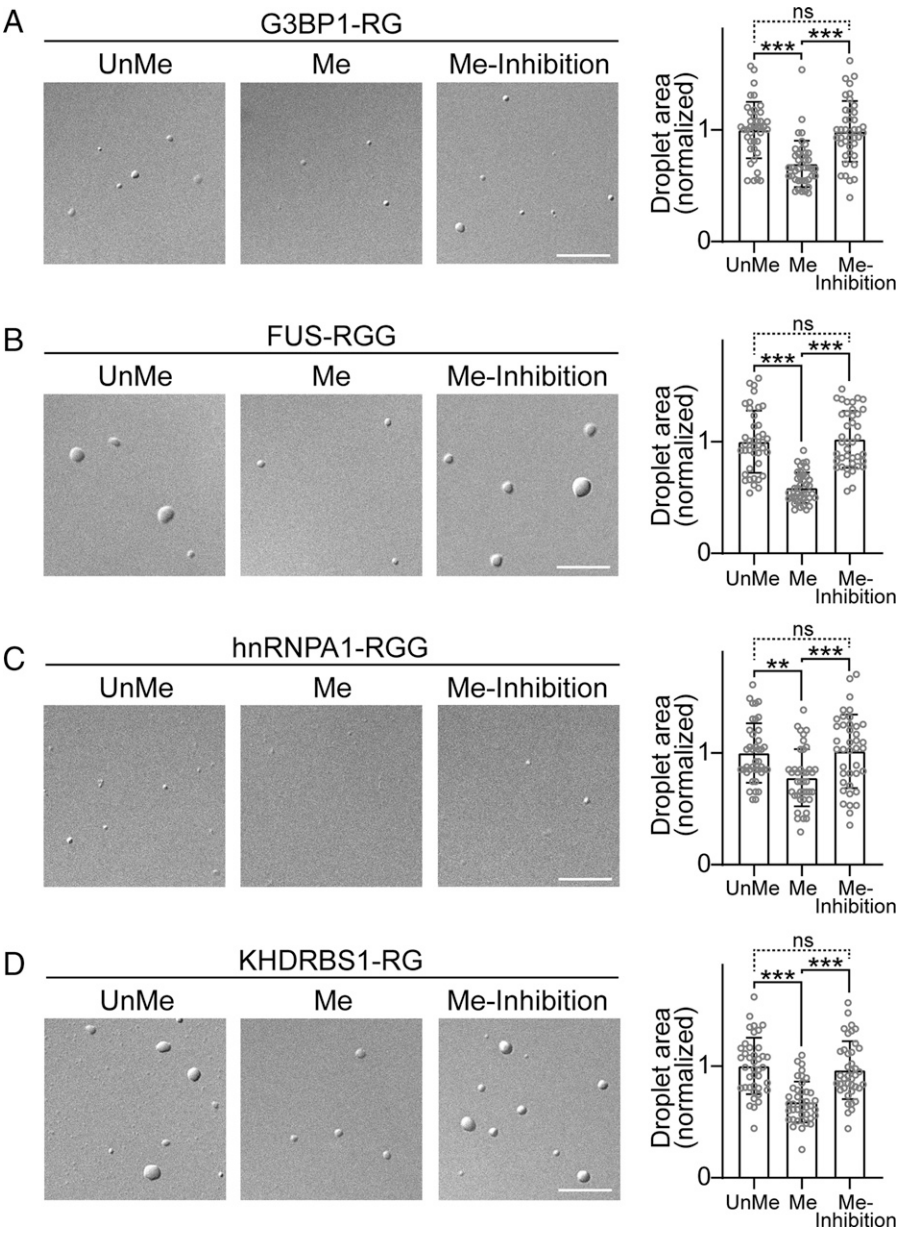

Fig. 6. Arginine methylation impairs the LLPS capability of the RG/RGG–rich region. (*A–D*) Observation and statistical analysis of liquid droplet formed by four RG/RGG–rich regions before and after arginine methylation. The methylated RG/RGG–rich regions in G3BP1, FUS, hnRNPA1, and KHDRBS1 were prepared as described in *Materials and Methods* and *SI Appendix*, Table S5. The differential interference contrast images of the droplets are shown on the *Left*, and the droplet area measurements on the *Right*. 'Me', arginine methylated RG/RGG–rich region. "UnMe" and "Me-Inhibition" are the controls (refer to *SI Appendix*, Table S5 for the detailed information). For each protein sample, the area of each droplet was normalized by the average droplet area of the "UnMe" sample. Error bars indicate SD, and each bar represents 40 droplets. $^{**}P < 0.01$, $^{***}P < 0.001$ by Student's *t* test. ns, nonsignificant difference. Scale bar: 10 μm.

arginine methylation forms including no methylation, MMA, aDMA, and sDMA, were prepared by treating four synthetic peptides (GGNFSGRGGFGGSR, GGNFSG-MMA-GGFGGSR, GGNFSG-aDMA-GGFGGSR, and GGNFSG-sDMA-GGFGGSR) with carboxypeptidase B (Sigma) at a peptide to enzyme ratio of 50:1 for 2 h at 50 °C. The primary amino groups in those peptides were dimethyl labeled (50) to prevent them from reacting with other chemical compounds. It is worth noting that the dimethyl group introduced by dimethyl labeling is on the N terminus or lysine residue, which is different from endogenous arginine dimethylation and does not interfere the DMA identification in this study. The peptide carrying sDMA was labeled by using formaldehyde-D_2 and sodium cyanoborodeuteride, but the other three peptides were labeled by using the nondeuterated reagents. All of the labeled peptides were desalted by using HLB cartridges, dried, and redissolved in water to a final concentration of 0.5 μg/μL. Then the peptides with unmethylated arginine, MMA, and one of DMAs were mixed at the mass ratio of 2:2:1, and 5 μg of peptide mixture was added into 50 μL of 200 mM NaOH water solution containing 20 mM 1,2-cyclohexanedione, and incubated at 37 °C for 40 min. Then the pH of the solution was adjusted to 7 by using 400 mM HCl. Agarose beads modified with *m*-aminophenylboronic acid (40 μL; Sigma) were washed with 3× 200 μL 0.1% formic acid (FA) and 3× 200 μL of 10 mM triethylammonium bicarbonate (TEAB) buffer (pH 10.0) and then added into the peptide mixture. Subsequently, 50 μL of 100 mM NaCl, 125 μL of 25 mM TEAB buffer (pH 10.2 to 10.4), and 1.54 μL of 40% pyruvic aldehyde solution (J&K) were added in sequence. The reaction was incubated at 15 °C for 1 h. Then the beads were filtered and washed with 3× 50 μL of 10 mM TEAB buffer (pH 10.0). Bound peptides were eluted by using 5× 50 μL of 0.1% FA. In each elution, the beads were incubated with 0.1% FA for 5 min. Eluted peptides were dried and redissolved in 1% $NH_3{\cdot}H_2O$ with 30% acetonitrile (ACN). The solution was incubated at room temperature (RT) for 1 h, and then the peptides were analyzed by MALDI MS.

We dissolved 100 μg of BSA in 100 μL of lysis buffer (100 mM Tris·HCl, 6 M guanidine hydrochloride, 10 mM tris(2-carboxyethyl)phosphine, and 40 mM chloroacetamide, pH 7.4) and heated at 100 °C for 5 min. After cooling, the

buffer was replaced with 100 mM Hepes (pH 7.9) by using a 10-KDa ultrafiltration tube. The alkylated BSA was digested by trypsin at 37 °C for 16 h. After digestion, the trypsin was removed by ultrafiltration. The tryptic digest was mixed with 1 μg of synthetic peptide, GGNFSG-R(me2a)-GGFGGSR or GGNFSG-R(me2s)-GGFGGSR. The peptide mixtures with aDMA or sDMA were dimethyl labeled by using nondeuterated and deuterated reagents, respectively. Labeled peptide mixtures were desalted, dried, and redissolved in 50 μL of 200 mM NaOH water solution containing 20 mM 1,2-cyclohexanedione; then both of the arginine dimethylated peptides were enriched as before.

Cell Culture, Small-Molecule Treatment, and SG Formation. For heavy methyl stable-isotope labeling by amino acid in cell culture (hM-SILAC), Roswell Park Memorial Institute (RPMI) medium 1640 lacking L-methionine (Gibco) was supplemented with 10% dialyzed fetal bovine serum (Gibco), 1% penicillin/streptomycin and 0.1mM either L-methionine or L-methionine-methyl-$^{13}CD_3$, DMEM (Gibco) lacking L-methionine, L-arginine, and L-lysine was supplemented with 10% dialyzed fetal bovine serum (Gibco), 1% penicillin/streptomycin, 0.398 mM L-arginine, 0.798 mM L-lysine, and 0.2 mM L-methionine-methyl-$^{13}CD_3$. Otherwise, cells were cultured in the medium supplemented with 10% fetal bovine serum and 1% penicillin/streptomycin. Jurkat T cells were cultured in the RPMI medium 1640, and HeLa cells in the DMEM. All the cells were grown at 37 °C in a humidified atmosphere with 5% CO_2. For hM-SILAC, cells were grown for seven cell doublings.

The HeLa cells treated with small molecules or stimulated by heat shock were not metabolically labeled. For small-molecule treatment, GSK591 and MS023 (Selleck) were used to treat HeLa cells at 5 μM and 10 μM for 48 h, respectively. To induce SG assembly, HeLa cells were treated with 200 μM $NaAsO_2$ or heated at 43 °C for 1 h. For SG disassembly, the medium containing sodium arsenite was removed and the cells were incubated in the fresh medium for 1 h.

Cell Lysis, Protein Digestion, and Peptide Labeling. Cells were mixed with the lysis buffer and heated at 100 °C for 5 min. The mixture was cooled on ice for 5 min and sonicated. The lysate was heated at 100 °C for 5 min, cooled, and centrifuged at 8,000*g* for 30 min at 4 °C. The supernatant was mixed with both 1× volume of 4 °C water and 8× volumes of −20 °C acetone, and incubated at −20 °C overnight. The precipitated protein was collected by centrifuging for 15 min at 2,000*g* and washed twice with −20 °C 80% acetone. The pellet was air-dried at RT for 10 min and mixed with digestion buffer (100 mM Hepes, pH 7.9). The precipitated protein was resuspended by sonicating.

Protein was digested by trypsin at 37 °C for 16 h. The trypsin was denatured by heating at 100 °C for 10 min. After cooling, the primary amino groups in part of the digest were blocked by dimethyl labeling in "light" form. The digest not blocked would be further digested by other proteases. In this situation, 2× Arg-C buffer (100 mM Hepes, 10 mM dithiothreitol [DTT], 0.4 mM EDTA, pH 7.65) and 500 mM $CaCl_2$ were added to the tryptic digest to a final concentration of 1× and 5 mM, respectively. Then the tryptic digest was further digested by Arg-C (Worthington Biochemical) at 37 °C for 16 h. To quench the DTT and denature the Arg-C, 500 mM chloroacetamide was added to a final concentration of 20 mM, and the solution was heated again at 100 °C for 10 min. After cooling, the peptides were digested by carboxypeptidase B at 50 °C for 2 h and blocked by dimethyl labeling as the tryptic digest. Finally, peptides were desalted by using HLB cartridge, and dried. The concentration of peptides was measured by nanodrop (Thermo Scientific).

Enrichment of Arginine Dimethylated Peptide from Whole-Protein Digest. We redissolved 100 μg of desalted peptides in 50 μL of 200 mM NaOH water solution with 20 mM 1,2-cyclohexanedione. Arginine dimethylated peptides were enriched as described earlier in *Materials and Methods*. After bound peptides were eluted from agarose beads and dried, they were redissolved in 60 μL of loading buffer (5 mM KH_2PO_4 buffer, pH 2.7, 20% ACN). The coeluted impurities, which are not peptides, were removed by strong cation exchange (SCX) chromatography, as described below. A small piece of degreasing cotton was packed into a 20-μL pipet tip. We added 5 μL of Polar MC30-SP SCX beads (Sepax) into the blocked tip and washed them with 3× 20 μL of elution buffer (1% $NH_3{\cdot}H_2O$, 30% ACN) and 6× 20 μL of loading buffer in sequence. Then the redissolved peptides were loaded on the beads. The beads were washed with 15 μL of wash buffer (0.01% trifluoroacetic acid [TFA], 30% ACN). Finally, bound peptides were eluted by using 3× 20 μL of elution buffer. The elution was incubated at RT for 1 h and dried.

Immunoaffinity enrichment of arginine dimethylated peptides was similar to the procedure previously described (31). Briefly, tryptic digest of 10 mg of whole proteins was dissolved in 1× immuno-affinity purification (IAP) buffer (9993, CST) and incubated with 80 μL of PTMscan Asymmetric Di-Methyl Arginine Motif antibody (13474, CST) or PTMscan Symmetric Di-Methyl Arginine Motif antibody (13563, CST) at 4 °C for 2 h on a rotator. When 200 μg of tryptic digest was used as starting material, 16 μL of antibody was used. Beads were centrifuged and washed two times in 1× IAP buffer and three times in water. The peptides in the beads were eluted by 0.15% TFA and desalted by C18. Finally, the peptides were digested again by trypsin for 2 h and desalted.

Basic Reverse-Phase LC for Fractionation. Basic reverse-phase LC for fractionation of peptide mixture was performed with a 4.6 × 250–mm analytical column containing 5 μm of C18 particles (ZORBAX 300Extend-C18, Agilent). The flow rate was set as 1 mL/min. The mobile-phases were as follows: phase A,5 mM ammonium bicarbonate in water (pH 8.0), and phase B, 25 mM ammonium bicarbonate in water (pH 8.0) with 80% ACN. The gradient was as follows: held at 2% B for 5 min, from 2% to 5% B in 1 min, from 5% to 10% B in 9 min, from 10% to 30% B in 60 min, from 30% to 40% B in 15 min, from 40% to 80% B in 5 min, and held at 80% B for 20 min. Carboxypeptidase B–treated peptides (1.1 mg) were fractionated. A total of 51 fractions from 19.5 min to 96 min were collected and further mixed into 17 fractions. These 17 fractions were dried and desalted. Arginine dimethylated peptides in each fraction were then enriched by SECEM.

MS Analysis. The mass shifts of synthetic peptides in different reactions were analyzed by an AB Sciex 5800 MALDI–time-of-flight/time-of-flight mass spectrometer with a pulsed Nd/YAG laser at 355 nm. We used 2,5-dihydroxybenzoic acid as a MALDI matrix. Peptide mixtures prepared from cells were analyzed by Q Exactive mass spectrometer (Thermo Scientific) equipped with the Ultimate 3000 RSLCnano System (Dionex). Peptides were redissolved in 0.1% FA and loaded on a 5-cm × 150-mm trap column (ReproSil-Pur 120C18, 1.9 μm). Then they were separated by using a linear gradient at 550 nL/min over 120 min in a 15-cm × 150-mm analytical column (ReproSil-Pur 120C18, 1.9 μm). In the mass spectrometer, survey scans (mass range, 300 to 1,750 Th) were acquired at a resolution of 70,000 at 200 Th. "Top 10" data-dependent acquisition mode was used with dynamic exclusion (30 s) for MS/MS scans. A 2-Th isolation window was used for higher-energy collisional dissociation fragmentation. MS/MS scans were acquired at a resolution of 35,000 at 200 Th.

Database Searching. MaxQuant (version 1.6.4.0) was used to search raw files against the Uniprot human database containing 20,361 entries (as of June 2018). When carboxypeptidase B was used, semispecific free C terminus of trypsin/P was set as digestion mode. A maximal of three miscleavages were allowed for the digestion mode of trypsin/P. For the database searching not to identify DMA, carbamidomethyl on cysteine and methyl-$^{13}CD_3$–labeled methionine were set as fixed modifications, while acetylation of protein N terminus and methionine oxidation were set as variable modifications. Other default parameters were not changed. To identify DMA, the dimethyl on the primary amino of peptide N terminus and lysine residue, carbamidomethyl on cysteine, and methyl-$^{13}CD_3$–labeled methionine were set as fixed modifications, while the spirocyclic group (C_6H_6O) on arginine residue and the "heavy" form of DMA were set as variable modifications. In particular, when dimethyl labeling was used in quantification, the dimethyl on the peptide N terminus and lysine residue were not set as fixed modifications. Water loss and ammonia loss were not be selected in the database searching. The false-discovery rates of PSM, protein, and site were set to the maximum. The cutoff score for modified peptides was 25. After the database searching, the identified arginine dimethylated peptides were further screened by the IonPEP algorithm.

IonPEP Algorithm. To control the confidence of arginine dimethylated peptide identification, posterior error probability (PEP), $p(X = false|n,I)$, was used. It was calculated by the following equation:

$$p(X = false|n, I) = \frac{p(n, I|X = false)p(X = false)}{p(n, I)}$$

To calculate the PEP of target PSM, the number of the matched daughter ions from this PSM and its peptide length were input as n and I, respectively. In the

dataset of all identified PSMs, the proportion of the PSMs whose peptide length and the number of matched daughter ions are equal to l and n, respectively, was used as the approximate value of $p(n,l)$. In the dataset of all reverse PSMs, the proportion was used as the approximate value of $p(n,l|X = false)$. $p(X = false)$ is the proportion of the reverse PSMs in all identified PSMs. By using the above equation, each PSM would have a PEP value reflecting its confidence. Then all PSMs were sorted by their PEP, starting with the minimum value. PSMs were accepted until the proportion of the reverse PSMs in all filtered PSMs was close to 1%. Because proline cannot be modified with two methyl groups, the PSM was removed when proline residue was presented in the peptide N terminus. For the samples that reacted with 1,2-cyclohexanedione, the PSMs identified with unmodified arginine were also removed. The DMA sites with a localization probability of <0.75 or identified as contaminant proteins were removed.

Bioinformatics Analysis. The LLPS-regulating protein database is located at lab.phasep.pro/. The RNA granule database is located at rnagranuledb.lunenfeld.ca/. IDRs were predicted by using IUPred3 (51). A sequence with the score of >0.5 was regarded as an IDR.

Methylproteome Analysis during SG Formation. When HeLa cells were metabolically labeled, they were cultured in the medium with dialyzed fetal bovine serum that did not have low-molecular-weight nutrients. Lacking these nutrients may influence SG formation. Thus, for the methylproteome analysis of SG formation, HeLa cells were not metabolically labeled. However, it would lead to the high false-positive rate of DMA identification. To control the identification confidence, we proposed the library-dependent quality control for methylproteome identification (Fig. 5*A*). First, by using SECEM, we built a library containing highly confident arginine dimethylated peptides identified from the HeLa cells metabolically labeled by heavy methionine. Then, the arginine dimethylated peptides identified in the methylproteome analysis of SG formation were matched with the library, and only the methylpeptides presented in the library would be considered in subsequent analysis.

In this study, stable-isotope dimethyl labeling was used to quantitatively investigate the dynamic change of DMA in the process of SG formation (50). Skyline was used to extract the MS1 peak areas of identified arginine dimethylated peptides (52). In the quantification, two samples with different states would be mixed at the mass ratio of 1:1; however, that ratio is always hard to reach. To calibrate the deviation, we also used stable-isotope dimethyl labeling to quantify the fold changes of whole proteins in the process of SG formation, calculated the median of these fold changes, and divided the fold change of each methylpeptide by this median. The calibrated value was regarded as the real fold change of methylpeptide.

Western Blot Analysis. After being treated with PRMT inhibitors or dimethyl sulfoxide (DMSO), HeLa cells were lysed in radioimmunoprecipitation assay buffer supplemented with a 1 mM mixture on ice. Lysates were clarified by centrifugation at 20,000*g* for 10 min. Protein concentration was determined using the BCA protein assay kit. Lysates were mixed with loading buffer, separated by 10% or 12% sodium dodecyl sulfate–polyacrylamide gel electrophoresis and transferred onto polyvinylidene difluoride membranes. The membranes were blocked and incubated with primary and secondary antibodies. Anti-asymmetric dimethylated arginine antibody (#13522), anti-symmetric dimethylated arginine antibody (#13222), and anti–β-actin antibody (#3700) were purchased from Cell Signaling Technology. The bands in the membranes were detected by BioImaging systems (Fusion FX5-XT).

Immunocytochemistry and Confocal Imaging. Cells were fixed with 4% paraformaldehyde in PBS for 15 min, permeabilized with 0.5% Triton X-100 in PBS for 10 min, and then blocked with 3% goat serum in PBST (PBS plus 0.1% Triton X-100) for 1 h, with all steps performed at RT. Cells were further incubated with anti–G3BP1 antibody (BD, 611127) overnight at 4 °C. AlexaFluor-488 (Invitrogen, A11001) used as the second antibody was incubated with the cells for 1 h at RT. After 3 washes with PBST, cells were mounted on glass slides using the ProLong Gold Antifade Mountant with DAPI (ThermoFisher, P36935). Images were captured using the Leica TCS SP8 confocal microscopy system with a ×100 objective (oil immersion). Images were processed and assembled into figures using LAS X (Leica) and Fiji.

Plasmid Construction and Protein Expression and Purification. For *E. coli* expression, G3BP1-RG (residues 411 to 466), FUS-RGG (residues 215 to 267), KHDRBS1-RG (residues 269 to 321), or their R-A mutants were cloned into pET28a with an N-terminal His-SUMO tag. HnRNPA1-RGG (residues 186 to 320) or its R-A mutant was cloned into a pET32a vector with an N-terminal Trx1 tag. For the R-A mutants, R447 and R460 of G3BP1-RG; R234, R242, and R244 of FUS-RGG; R284, R289, and R291 of KHDRBS1-RG; and R196, R206, and R218 of hnRNPA1-RGG were mutated. The tyrosine-rich region of FUS (residues 1 to 163) was cloned into pET22b with an N-terminal His tag. The tyrosine-rich region of KHDRBS1 (residues 269 to 443) was cloned into pET28a with an N-terminal His-SUMO tag. ULP1 (residues 403 to 621) was cloned into pET28a with an N-terminal His tag. Prmt1 (rat, residues 1 to 353) was cloned into pGEX-6P-1 vector with an N-terminal GST tag. All recombinant plasmids were validated by sequencing.

For protein purification, all plasmids were overexpressed in *E. coli* BL21(DE3) with induction of 0.5 mM isopropyl β-d-1-thiogalactopyranoside (IPTG) at 16 °C for 16 h except that hnRNPA1 and its mutant were overexpressed with induction of 0.4 mM IPTG at 25 °C for 12 h. After G3BP1-RG, FUS-RGG, KHDRBS1-RG, their R-A mutants, the tyrosine-rich region of KHDRBS1 or ULP1 expression, cells were harvested and lysed in 50 mM Tris·HCl (pH 7.5), 500 mM NaCl, 25 mM imidazole, 2 mM β-mercaptoethanol, and 2 mM phenylmethylsulfonyl fluoride (PMSF) at 4 °C. Proteins were purified by using an Ni column and eluted by the buffer containing 50 mM Tris·HCl (pH 7.5), 500 mM NaCl, 500 mM imidazole, and 4 mM β-mercaptoethanol. Eluted proteins were fractionated via Superdex 75 16/600 column in 50 mM Tris·HCl (pH 7.5), 100 mM NaCl, and 2 mM DTT.

After hnRNPA1-RGG or its R-A mutant expression, cells were harvested and lysed in bacteria lysis buffer (50 mM Tris·HCl, 6 M guanidine hydrochloride, pH 8.0) at RT. Proteins were purified by using an Ni column and eluted by the buffer containing 50 mM Tris·HCl (pH 8.0), 6 M guanidine hydrochloride, and 500 mM imidazole. Proteins then were further purified by C18 column (Phenomenex 00G-4053-N0) and dried. Trx1 tags in two proteins were cleaved by 3C enzyme at a molar ratio of 50:1 at RT overnight. Then the precipitates were collected by centrifugation at 3,724*g* for 30 min at RT and dissolved in bacteria lysis buffer. HnRNPA1-RGG or its mutant without tag was purified by C18 column again.

After the tyrosine-rich region of FUS expression, cells were harvested and lysed in bacteria lysis buffer at RT. The protein was purified by using an Ni column and eluted by the buffer containing 50 mM Tris·HCl (pH 8.0), 6 M guanidine hydrochloride, and 500 mM imidazole. Then the buffer was changed to 5 mM *N*-cyclohexyl-3-aminopropanesulfonic acid (pH 11) by desalting column.

After Prmt1 expression, cells were harvested and lysed in 50 mM Tris·HCl (pH 8.0), 500 mM NaCl, and 2 mM PMSF at 4 °C. Protein was purified using a GST column and eluted by the buffer containing 20 mM Tris·HCl (pH 8.0), 50 mM NaCl, and 20 mM GSH. Then the buffer was changed to 20 mM Tris·HCl (pH 8.0) and 50 mM NaCl by dialysis.

In Vitro Arginine Methylation Assay. Purified G3BP1-RG, FUS-RGG, KHDRBS1-RG, or hnRNPA1-RGG was mixed with other substrates as described in the *SI Appendix*, Table S5. These samples were prepared in the buffer containing 20 mM Tris·HCl (pH 8.0), 5% (vol/vol) glycerol, 1 mM EDTA, and 1 mM DTT. The final concentration of the purified protein in each sample was 50 μM. Prmt1 and MS023 were added at a final concentration of 50 μM, respectively, and *S*-adenosylmethionine was added at a final concentration of 0.5 mM. Then all of samples were incubated at 37 °C overnight. After the incubation, NaCl was added to a final concentration of 200 mM for the sample containing G3BP1-RG, FUS-RGG, or KHDRBS1-RG. Then these proteins were incubated with ULP1 (molar ratio of 1:1) at 37 °C for 1 h to cut off His-SUMO tags. Prmt1 and ULP1 in all samples were precipitated by boiling at 90 °C for 10 min and removed by centrifugation at 14,000*g* for 10 min.

In Vitro LLPS Assay. To determine the influence of the mutated sites on protein LLPS, G3BP1-RG (2 mg/mL), FUS-RGG (1.9 mg/mL), KHDRBS1-RG (1 mg/mL), hnRNPA1-RGG (0.6 mg/mL), and their mutants were prepared in the buffer containing 50 mM Tris·HCl (pH 7.5), 1 mM DTT, and 100 mM NaCl in the water solution containing 10% (wt/vol) polyethylene glycol 3,350. In vitro LLPS experiments were performed at RT.

To determine the influence of arginine methylation on protein LLPS, unmethylated or methylated proteins, including G3BP1-RG (0.6 mg/mL), FUS-RGG (0.5 mg/mL), and hnRNPA1-RGG (0.6 mg/mL), were prepared with the tyrosine-rich region of FUS (0.9 mg/mL) to trigger phase separation. The unmethylated or methylated KHDRBS1-RG (0.6 mg/mL) was prepared with the tyrosine-rich region of KHDRBS1 (0.6 mg/mL). These samples were prepared in the buffer containing 20 mM Tris·HCl (pH 8.0), 200 mM NaCl, 5% (vol/vol) glycerol, 1 mM EDTA, and 1 mM DTT. Of note, addition of the tyrosine-rich region of FUS or KHDRBS1 into the protein phase-separation assays of the protein samples from in vitro arginine methylation assays is to enhance LLPS of the four RG/RGG regions, since we found the procedure for sample preparation of in vitro arginine methylation (e.g., methylation, heating, centrifugation) generally decreases LLPS capability of the four RG/RGG regions. In vitro LLPS experiments were all performed at RT.

All images were captured within 5 min after LLPS induction. Differential interference contrast images of droplets were acquired on a Leica TCS SP8 microscope with a ×100 objective (oil immersion) at a resolution of 2,048 × 2,048 pixels after 3 μL of sample was pipetted onto a glass slide and coverslip sealed. The optical density at 600 nm of samples was measured by a Varioskan Flash spectral scanning multimode reader (Thermo Fisher). Droplet areas were measured by Image J software.

Data, Materials, and Software Availability. Mass spectrometry data are available via ProteomeXchange with the identifier PXD033048 (53) and PXD035137 (54). All other data are included in the article and/or *SI Appendix*.

ACKNOWLEDGMENTS. This work was supported, in part, by the National Key Research and Development Program of China (grants 2021YFA1302602, 2020YFE0202200, and 2019YFE0120600), the National Natural Science Foundation of China (grants 21974045, 91753105, 92153302, 82188101, 32170683, 31872716, and 32171236), the innovation program (DICP & QIBEBT UN201802) of science and research from the DICP, CAS, and Innovation Academy for Precision Measurement Science and Technology, CAS, the Science and Technology Commission of Shanghai Municipality (grants 20XD1425000 and 2019SHZDZX02), the Shanghai Pilot Program for Basic Research, Chinese Academy of Science, Shanghai Branch (grant CYJ-SHFY-2022-005).

Author affiliations: [a]Chinese Academy of Sciences Key Laboratory of Separation Sciences for Analytical Chemistry, National Chromatographic R&A Center, Dalian Institute of Chemical Physics, Chinese Academy of Sciences, Dalian 116023, China; [b]University of Chinese Academy of Sciences, Beijing 100049, China; [c]Shanghai Key Laboratory of Functional Materials Chemistry, Department of Chemistry and Molecular Engineering, East China University of Science and Technology, Shanghai 200237, China; [d]Bio-X Institutes, Key Laboratory for the Genetics of Developmental and Neuropsychiatric Disorders, Ministry of Education, Shanghai Jiao Tong University, Shanghai 200030, China; [e]Zhangjiang Institute for Advanced Study, Shanghai Jiao Tong University, Shanghai 200240, China; [f]Interdisciplinary Research Center on Biology and Chemistry, Shanghai Institute of Organic Chemistry, Chinese Academy of Sciences, Shanghai 201210, China; and [g]State Key Laboratory of Bio-Organic and Natural Products Chemistry, Shanghai Institute of Organic Chemistry, University of Chinese Academy of Sciences, Shanghai 200032, China

Author contributions: Q.W., Z. Li, S.Z., Y.W., C.L., and M.Y. designed research; Q.W., Z. Li, S.Z., Y.L., Y.M., Z. Liu, C.L., and M.Y. performed research; Q.W., Z. Li, S.Z., C.L., and M.Y. contributed new reagents/analytic tools; Q.W., S.Z., Z.F., W.Z., D.L., C.L., and M.Y. analyzed data; and Q.W., C.L., and M.Y. wrote the paper.

1. R. S. Blanc, S. Richard, Arginine methylation: The coming of age. *Mol. Cell* **65**, 8–24 (2017).
2. J. Murn, Y. Shi, The winding path of protein methylation research: Milestones and new frontiers. *Nat. Rev. Mol. Cell Biol.* **18**, 517–527 (2017).
3. E. Guccione, S. Richard, The regulation, functions and clinical relevance of arginine methylation. *Nat. Rev. Mol. Cell Biol.* **20**, 642–657 (2019).
4. Y. Yang, M. T. Bedford, Protein arginine methyltransferases and cancer. *Nat. Rev. Cancer* **13**, 37–50 (2013).
5. S. M. Greenblatt, F. Liu, S. D. Nimer, Arginine methyltransferases in normal and malignant hematopoiesis. *Exp. Hematol.* **44**, 435–441 (2016).
6. M. L. Tradewell *et al.*, Arginine methylation by PRMT1 regulates nuclear-cytoplasmic localization and toxicity of FUS/TLS harbouring ALS-linked mutations. *Hum. Mol. Genet.* **21**, 136–149 (2012).
7. M. Suárez-Calvet *et al.*, Monomethylated and unmethylated FUS exhibit increased binding to Transportin and distinguish FTLD-FUS from ALS-FUS. *Acta Neuropathol.* **131**, 587–604 (2016).
8. M. Hofweber *et al.*, Phase separation of FUS is suppressed by its nuclear import receptor and arginine methylation. *Cell* **173**, 706–719.e13 (2018).
9. S. Qamar *et al.*, FUS phase separation is modulated by a molecular chaperone and methylation of arginine cation-π interactions. *Cell* **173**, 720–734.e15 (2018).
10. V. H. Ryan *et al.*, Mechanistic view of hnRNPA2 low-complexity domain structure, interactions, and phase separation altered by mutation and arginine methylation. *Mol. Cell* **69**, 465–479.e7 (2018).
11. W. C. Tsai *et al.*, Arginine demethylation of G3BP1 promotes stress granule assembly. *J. Biol. Chem.* **291**, 22671–22685 (2016).
12. S. Boeynaems *et al.*, Protein phase separation: A new phase in cell biology. *Trends Cell Biol.* **28**, 420–435 (2018).
13. G. Zhang, Z. Wang, Z. Du, H. Zhang, mTOR regulates phase separation of PGL granules to modulate their autophagic degradation. *Cell* **174**, 1492–1506.e22 (2018).
14. T. J. Nott *et al.*, Phase transition of a disordered nuage protein generates environmentally responsive membraneless organelles. *Mol. Cell* **57**, 936–947 (2015).
15. M. Hofweber, D. Dormann, Friend or foe–post-translational modifications as regulators of phase separation and RNP granule dynamics. *J. Biol. Chem.* **294**, 7137–7150 (2019).
16. T. Uhlmann *et al.*, A method for large-scale identification of protein arginine methylation. *Mol. Cell. Proteomics* **11**, 1489–1499 (2012).
17. M. Bremang *et al.*, Mass spectrometry-based identification and characterisation of lysine and arginine methylation in the human proteome. *Mol. Biosyst.* **9**, 2231–2247 (2013).
18. A. Guo *et al.*, Immunoaffinity enrichment and mass spectrometry analysis of protein methylation. *Mol. Cell. Proteomics* **13**, 372–387 (2014).
19. V. Geoghegan, A. Guo, D. Trudgian, B. Thomas, O. Acuto, Comprehensive identification of arginine methylation in primary T cells reveals regulatory roles in cell signalling. *Nat. Commun.* **6**, 6758 (2015).
20. K. Wang *et al.*, Antibody-free approach for the global analysis of protein methylation. *Anal. Chem.* **88**, 11319–11327 (2016).
21. Q. Wang, K. Wang, M. Ye, Strategies for large-scale analysis of non-histone protein methylation by LC-MS/MS. *Analyst (Lond.)* **142**, 3536–3548 (2017).
22. Q. Wang, Z. Liu, K. Wang, Y. Wang, M. Ye, A new chromatographic approach to analyze methylproteome with enhanced lysine methylation identification performance. *Anal. Chim. Acta* **1068**, 111–119 (2019).
23. Q. Wang *et al.*, Chemical depletion of histidine-containing peptides allows identification of more low-abundance methylation sites from proteome samples. *J. Proteome Res.* **20**, 2497–2505 (2021).
24. D. Li, Y. Chen, Z. Liu, Boronate affinity materials for separation and molecular recognition: Structure, properties and applications. *Chem. Soc. Rev.* **44**, 8097–8123 (2015).
25. A. Leitner, W. Lindner, Probing of arginine residues in peptides and proteins using selective tagging and electrospray ionization mass spectrometry. *J. Mass Spectrom.* **38**, 891–899 (2003).
26. A. Foettinger, A. Leitner, W. Lindner, Solid-phase capture and release of arginine peptides by selective tagging and boronate affinity chromatography. *J. Chromatogr. A* **1079**, 187–196 (2005).
27. E. L. Smith, Reversible blocking at arginine by cyclohexanedione. *Methods Enzymol.* **47**, 156–161 (1977).
28. G. Hart-Smith, D. Yagoub, A. P. Tay, R. Pickford, M. R. Wilkins, Large scale mass spectrometry-based identifications of enzyme-mediated protein methylation are subject to high false discovery rates. *Mol. Cell. Proteomics* **15**, 989–1006 (2016).
29. S. E. Ong, G. Mittler, M. Mann, Identifying and quantifying in vivo methylation sites by heavy methyl SILAC. *Nat. Methods* **1**, 119–126 (2004).
30. S. C. Larsen *et al.*, Proteome-wide analysis of arginine monomethylation reveals widespread occurrence in human cells. *Sci. Signal.* **9**, rs9 (2016).
31. N. G. Hartel, B. Chew, J. Qin, J. Xu, N. A. Graham, Deep protein methylation profiling by combined chemical and immunoaffinity approaches reveals novel PRMT1 targets. *Mol. Cell. Proteomics* **18**, 2149–2164 (2019).
32. P. Thandapani, T. R. O'Connor, T. L. Bailey, S. Richard, Defining the RGG/RG motif. *Mol. Cell* **50**, 613–623 (2013).
33. P. A. Chong, R. M. Vernon, J. D. Forman-Kay, RGG/RG motif regions in RNA binding and phase separation. *J. Mol. Biol.* **430**, 4650–4665 (2018).
34. S. Boeynaems *et al.*, Phase separation of C9orf72 dipeptide repeats perturbs stress granule dynamics. *Mol. Cell* **65**, 1044–1055.e5 (2017).
35. S. Elbaum-Garfinkle *et al.*, The disordered P granule protein LAF-1 drives phase separation into droplets with tunable viscosity and dynamics. *Proc. Natl. Acad. Sci. U.S.A.* **112**, 7189–7194 (2015).
36. S. Saha *et al.*, Polar positioning of phase-separated liquid compartments in cells regulated by an mRNA competition mechanism. *Cell* **166**, 1572–1584.e1516 (2016).
37. Y.-H. Lin, J. D. Forman-Kay, H. S. Chan, Theories for sequence-dependent phase behaviors of biomolecular condensates. *Biochemistry* **57**, 2499–2508 (2018).
38. T. Mittag, R. Parker, Multiple modes of protein-protein interactions promote RNP granule assembly. *J. Mol. Biol.* **430**, 4636–4649 (2018).
39. E. W. Martin, A. S. Holehouse, Intrinsically disordered protein regions and phase separation: Sequence determinants of assembly or lack thereof. *Emerg. Top. Life Sci.* **4**, 307–329 (2020).
40. K. You *et al.*, PhaSepDB: A database of liquid-liquid phase separation related proteins. *Nucleic Acids Res.* **48** (D1), D354–D359 (2020).
41. J. Y. Youn *et al.*, Properties of stress granule and P-body proteomes. *Mol. Cell* **76**, 286–294 (2019).
42. P. Yang *et al.*, G3BP1 is a tunable switch that triggers phase separation to assemble stress granules. *Cell* **181**, 325–345.e28 (2020).
43. J. Guillén-Boixet *et al.*, RNA-induced conformational switching and clustering of G3BP drive stress granule assembly by condensation. *Cell* **181**, 346–361.e17 (2020).
44. D. W. Sanders *et al.*, Competing protein-RNA interaction networks control multiphase intracellular organization. *Cell* **181**, 306–324.e28 (2020).
45. A. C. Murthy *et al.*, Molecular interactions contributing to FUS SYGQ LC-RGG phase separation and co-partitioning with RNA polymerase II heptads. *Nat. Struct. Mol. Biol.* **28**, 923–935 (2021).
46. A. Molliex *et al.*, Phase separation by low complexity domains promotes stress granule assembly and drives pathological fibrillization. *Cell* **163**, 123–133 (2015).
47. J. Henao-Mejia *et al.*, Suppression of HIV-1 Nef translation by Sam68 mutant-induced stress granules and nef mRNA sequestration. *Mol. Cell* **33**, 87–96 (2009).
48. J. Henao-Mejia, J. J. He, Sam68 relocalization into stress granules in response to oxidative stress through complexing with TIA-1. *Exp. Cell Res.* **315**, 3381–3395 (2009).
49. H. H. Wei *et al.*, A systematic survey of PRMT interactomes reveals the key roles of arginine methylation in the global control of RNA splicing and translation. *Sci. Bull. (Beijing)* **66**, 1342–1357 (2021).

50. J. L. Hsu, S. Y. Huang, N. H. Chow, S. H. Chen, Stable-isotope dimethyl labeling for quantitative proteomics. *Anal. Chem.* **75**, 6843–6852 (2003).
51. G. Erdős, M. Pajkos, Z. Dosztányi, IUPred3: Prediction of protein disorder enhanced with unambiguous experimental annotation and visualization of evolutionary conservation. *Nucleic Acids Res.* **49** (W1), W297–W303 (2021).
52. B. MacLean *et al.*, Skyline: An open source document editor for creating and analyzing targeted proteomics experiments. *Bioinformatics* **26**, 966–968 (2010).
53. Q. Wang *et al*., Global profiling of arginine dimethylation in regulating protein phase separation by a steric effect–based chemical-enrichment method. ProteomeXchange. http://proteomecentral.proteomexchange.org/cgi/GetDataset?ID=PXD033048. Deposited 7 April 2022.
54. Q. Wang *et al*., Global profiling of arginine dimethylation in regulating protein phase separation by a steric effect–based chemical-enrichment method. ProteomeXchange. http://proteomecentral.proteomexchange.org/cgi/GetDataset?ID=PXD035137. Deposited 7 July 2022.